

A High-Sensitivity Fully-Passive Neurosensing System for Wireless Brain Signal Monitoring

Cedric W. L. Lee, *Student Member, IEEE*, Asimina Kiourti, *Member, IEEE*, Junseok Chae, *Senior Member, IEEE* and John L. Volakis, *Fellow, IEEE*

Abstract—A high-sensitivity, fully-passive neurosensing system is presented for wireless brain signal monitoring. The proposed system is able to detect very low power brain-like signals, viz. as low as -82 dBm ($50 \mu\text{V}_{\text{pp}}$) at $f_{\text{neuro}} > 1 \text{ kHz}$. It is also able to read emulated neural signals as low as -70 dBm ($200 \mu\text{V}_{\text{pp}}$) at $f_{\text{neuro}} > 100 \text{ Hz}$. This is an improvement of up to 22 dB in sensitivity as compared to previously reported neural signals. The system is comprised of an implanted neurosensor and an exterior interrogator. The neurosensor receives an external carrier signal and mixes it with the neural signals prior to retransmitting to the interrogator. Of importance is that the implanted neurosensor is fully passive and does not require a battery nor rectifier/regulator, but is concurrently wireless for unobtrusive neurosensing with minimal impact to the individual’s activity. To achieve this remarkable high sensitivity, the sensing system employed: (a) a sub-harmonic mixer using an anti-parallel diode pair (APDP), (b) a pair of implanted/interrogator antennas with high transmission coefficient, $|S_{21}|$, and (c) a matching circuit between the implanted antenna and the mixer. This neurosensing system brings forward a new possibility of wireless neural signal detection using passive brain implants.

Index Terms—Anti-parallel diode pair (APDP), brain implant, neurosensing, passive, wireless medical telemetry, sub-harmonic mixing.

I. INTRODUCTION

BRAIN implant technology has the potential to improve the individual’s well-being. Example applications include early detection of epileptic seizures, behavioral studies to assess levels of consciousness (e.g., during sleep, anesthesia or brain injury), understanding and improving the brain’s functionality for the aging, people with Alzheimer’s and people with mental disorders, etc [1]-[6]. However, development of this promising technology has been challenging because of three major concerns. Specifically, so far, wires have been used to connect the intra-cranial implants to the exterior interrogator units [7]. As would be expected,

Manuscript received June 16, 2014; revised March 27, 2015. This material is based upon work supported by the National Science Foundation under Grant No. 1344825.

C. W. L. Lee, A. Kiourti, and J. L. Volakis are with the ElectroScience Laboratory, Department of Electrical & Computer Engineering, The Ohio State University, Columbus, OH 43212 USA (e-mail: lee.6256@osu.edu; kiourti.1@osu.edu; volakis.1@osu.edu).

J. Chae is with the School of Electrical, Computer, and Energy Engineering, Arizona State University, Tempe, AZ 85287 USA (e-mail: Junseok.Chae@asu.edu).

TABLE I
VOLTAGE AND FREQUENCY RANGE OF SIGNALS GENERATED BY THE HUMAN BRAIN

Neural signals	Voltage Range	Frequency Range
ElectroCorticographic (ECoG) signals	100 – 200 μV_{pp}	< 500 Hz
Neural “spikes”	100 – 2000 μV_{pp}	300 Hz – 5 kHz
Local Field Potentials (LFPs)	20 – 2000 μV_{pp}	< 500 Hz

such sensors imply severe restrictions to the physical movements of the patients, and endanger their safety. Another issue is the heat generated by the employed dense electronics [8] [9]. This heating might disturb normal brain operation and damage the cerebral tissue. Also, use of a battery for the implant is unattractive as its replacement requires multiple invasive surgical operations to replace it.

In terms of past research efforts for brain signal detection, RFID-based ElectroEncephaloGram (EEG) [10], and mm-size neural tags for RFID-inspired wireless brain-machine interfaces [11][12] have been employed. The former are wearable, implying that only EEG signals at the surface of the human scalp may be acquired. However, they are limited in providing highly localized information about the brain activity. By contrast, implanted electrodes inside the skull have been found to be more effective [13]. The latter tags are intended for brain implants and consist of the antenna and an array of electrodes with ultra-low-power integrated circuits (IC). Though use of a battery has been avoided, an RF-to-DC converter and storage device are still needed to power the IC. Therefore, these implants, although passive, are not fully-passive.

As an alternative to the above, in [14] and [15] we considered fully-passive and wireless implants. Specifically, the term “fully-passive” implies that no battery, no energy harvesting unit, and no rectifier/regulator are included. This type of passive and wireless acquisition of neural signals has the unique property of very minor heating, thus, minimizing injury and trauma to the brain while preserving natural lifestyle and comfort. However, the minimum detectable signal reported so far for neurosensors was $6000 \mu\text{V}_{\text{pp}}$ (-40 dBm) at $f_{\text{neuro}} = 400 \text{ Hz}$ [15], $1125 \mu\text{V}_{\text{pp}}$ (-55 dBm) at $f_{\text{neuro}} = 400 \text{ Hz}$ [14], and $500 \mu\text{V}_{\text{pp}}$ (-62 dBm) at $f_{\text{neuro}} = 140 \text{ Hz}$ [14]. These levels are not in a range to properly detect typical neural signal signals. Specifically, as summarized in Table I, the amplitude of human ElectroCorticoGraphic (ECoG)

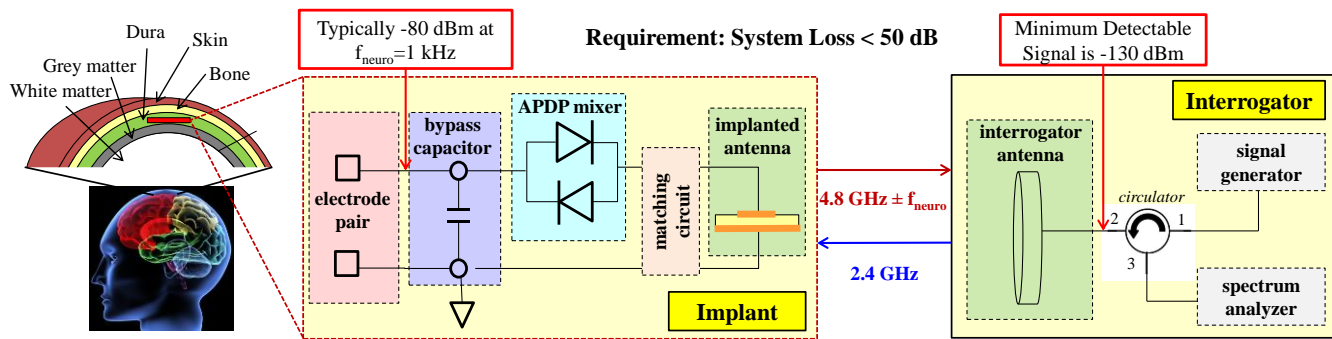


Fig. 1. Block diagram of the proposed wireless neurosensing system.

recordings is on the order of $100 - 200 \mu\text{V}_{\text{pp}}$ [16]. Additionally, neural “spikes” often appear in the $300\text{ Hz} - 5\text{ kHz}$ frequency range with amplitudes of $100 - 2000 \mu\text{V}_{\text{pp}}$. These arise and are typically acquired as voltages generated by active neurons [17] [18]. Also, low-frequency ($< 200\text{ Hz}$) oscillations exist with amplitudes of $20 - 2000 \mu\text{V}_{\text{pp}}$, known as Local Field Potentials (LFPs) [19]. The latter originate from the collective and synchronous action of thousands of relatively distant neurons. Therefore, the neurosensor reported in [14] cannot read typical ECoG signals. It can only detect a certain portion of neural “spikes” and LFPs.

This paper builds upon the aforementioned concept to design a new and improved fully-passive and wireless neurosensing system. This new neurosensing system demonstrates that brain-like signals as low as $50 \mu\text{V}_{\text{pp}}$ can be detected. Preliminary results were recently given by the authors in the conference paper [20]. Specifically, it is demonstrated that the new wireless neurosensor can detect signals down to -82 dBm ($50 \mu\text{V}_{\text{pp}}$) at $f_{\text{neuro}} = 1\text{ kHz}$. This is achieved by minimizing propagation and circuit losses down to $< 50\text{ dB}$. This implies a detectable signal of -130 dBm [21] [22] using commercial electronics. Of importance is that this type of passive operation eliminates use of bulky power supplies (i.e., batteries) and reduces circuit complexity. It also avoids possible power failures and significantly reduces power dissipation. Concurrently, wireless connectivity lowers the risk of infections and allows for unobtrusive sensing of brain signals with minimum impact to the individual’s activity.

This paper is organized as follows. Section II presents an overview of the proposed neurosensing system. Section III gives the design details and performance of the system components. Section IV assesses the performance of the overall neurosensing system in wireless configuration for brain signal monitoring.

II. SYSTEM OPERATION

The block diagram of the proposed neurosensing system is shown in Fig. 1. It consists of two sub-systems: (1) the neurosensor to be implanted just below the dura, and above the grey matter of the human brain [15] [23], and (2) the exterior interrogator, placed right outside the scalp and can be embedded with a typical baseball cap or incorporated within a textile band. The implant would detect the neural signals at

f_{neuro} via a pair of microelectrodes. Like in radio transmission, to read these signals by the interrogator (receiver), they are first mixed with a carrier signal prior to transmission. The carrier frequency was selected to be $f_c = 2.4\text{ GHz}$ that lies within the Industrial, Scientific and Medical (ISM) applications band [24]. This carrier is generated by the interrogator and transmitted wirelessly to the implant for mixing. When received by the implanted antenna, the 2.4 GHz carrier signal serves to activate the neurosensor and turn “ON” the mixer diodes. For isolation between the transmit and receive signals, the mixed signals were chosen across the carrier’s second harmonic at $4.8\text{ GHz} \pm f_{\text{neuro}}$ for transmission back to the interrogator. Generation of the second harmonic can be performed very efficiently by employing an anti-parallel diode pair (APDP) mixer circuit (see Fig. 1). The latter allows for efficient harmonic mixing since both the negative and positive legs of the 2.4 GHz signal are captured. This is a very attractive feature of the proposed system because harmonic mixing introduces only a very low conversion loss and is discussed in Section III.A. For comparison, the mixer configuration employed in [14] did not use both legs of the carrier. As a result, its sensitivity was lower. We note that the idea of using higher-order harmonics has been employed in the past for automotive vehicle [25], insect tracking [26], and RFID [27] applications. However, herewith, we employ the APDP mixer to minimize losses in biomedical applications, and specifically in fully-passive and wireless medical implants.

A critical component of the proposed implant is the bypass capacitor, placed between the implanted electrodes and mixer, as shown in Fig. 1. At high frequencies (2.4 GHz), the bypass capacitor acts as a short-circuit. As such, the carrier signal is allowed to reach the mixer ports, turn “ON” the diodes and activate normal mixing operation. Concurrently, it prevents excess high-frequency currents from flowing into the brain, thus preserving the integrity of the neurons. At low frequencies (f_{neuro}), the bypass capacitor acts as an open-circuit. In doing so, the brain neural signals (f_{neuro}) are allowed to reach the mixer ports. After mixing, the modulated ($4.8\text{ GHz} \pm f_{\text{neuro}}$) signal is wirelessly transmitted to the exterior interrogator via the implanted antenna. For optimum power transfer, a matching circuit is placed between the

implanted mixer and antenna. It is important to note that the electrodes used to detect the neural signal and the underlying tissue interface are associated with high impedances [17]. Also, these impedances vary dynamically, and are hard to predict [17]. Thus, the input impedance of the implanted circuit looking from the electrodes side must be high. This will allow effective transfer of neural signals to the mixer. To address this issue, a patch was selected as the implanted dual-band antenna. At low frequencies (f_{neuro}), the patch antenna acts as a capacitor, and therefore, the electrodes see an open-circuit (high impedance). Of course, the matching circuit has to be designed accordingly. For example, the matching circuit cannot include only shunt inductors; the latter would short-circuit the implanted antenna and lower the input impedance of the implant, looking in from the electrodes port.

At the interrogator side, a wideband spiral antenna is employed that operates from 0.6 GHz to 6 GHz [28] [29]. The low-profile property of the spiral antenna enhances its near field coupling with the implanted patch antenna. As such, the transmission coefficient, $|S_{21}|$, is maximized. This is crucial in reducing the overall system loss and improving the system sensitivity. As would be expected, the receiving section of the interrogator may include a demodulator to remove the 4.8 GHz frequency component and extract the neural signals at around f_{neuro} .

III. NEUROSENSING SYSTEM COMPONENTS

The goal in designing and choosing the transceiver components of the neurosensor in Fig. 1 is to keep losses at a minimum. These losses mainly come from two segments: (a) conversion loss of the implanted mixer, and (b) wireless propagation loss (i.e., antenna gain and path loss). Therefore, to improve the sensitivity of the overall system, both of these sources of loss must be accounted for. In the following, both of these issues are discussed, along with the implanted mixer and implanted antenna choices.

The proposed transceiver should be able to read typical low-level neural signals of < -80 dBm ($< 63 \mu\text{V}_{\text{pp}}$) at $f_{\text{neuro}} = 1$ kHz. The latter is a typical frequency of the neural signals, and has been a characteristic neural-activity-related frequency, often used for system benchmarking [14]. As the minimum detectable signal (MDS_{Rx}) is -130 dBm at our receiver, the aforementioned specification implies a system loss of < 50 dB at $f_{\text{neuro}} = 1$ kHz (see Fig. 1). To achieve this, the mixer and propagation loss must each have < 25 dB of loss at $f_{\text{neuro}} = 1$ kHz. The aforementioned estimates are based on a stipulated neural signal bandwidth of $\text{BW}_{\text{IF}} = 5$ kHz (see Table 1), a receiver noise figure of $\text{NF}_{\text{RX}} = 4$ dB, and an allowance of 3 dB above the noise floor for detection. Specifically [30]:

$$\begin{aligned} \text{MDS}_{\text{Rx}} &= kT + 10 \log \text{BW}_{\text{IF}} + \text{NF}_{\text{RX}} + 3 \text{dB} = \\ &= -174 \text{ dBm/Hz} + 37 \text{ dB} + 4 \text{ dB} + 3 \text{ dB} = \\ &= -130 \text{ dBm} \end{aligned} \quad (1)$$

where $kT = -174$ is the thermal noise power in dBm per 1 Hz of bandwidth at room temperature.

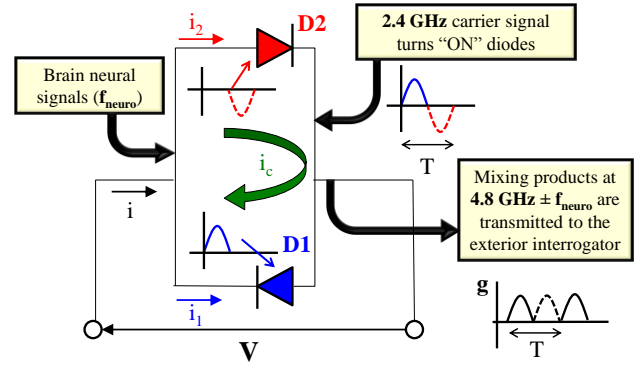


Fig. 2. Operation of the anti-parallel diode pair (APDP) as a sub-harmonic mixer for brain neurosensing applications.

A. Implanted Mixer

1) Implanted mixer operation

An attractive feature of the mixer circuit is the anti-parallel diode pair (APDP) mixing configuration (Fig. 1). The mixer serves to perform harmonic mixing at twice the carrier frequency ($2 \cdot f_c = 4.8$ GHz). Doing so allows for transmission back to the interrogator at $4.8 \text{ GHz} \pm f_{\text{neuro}}$.

To describe the above mixing operations, let us first consider the instantaneous currents through the diodes D1 and D2 in Fig. 2, which are [31]-[33]:

$$i_1 = -i_s(e^{-\alpha V} - 1) \quad (2)$$

$$i_2 = i_s(e^{\alpha V} - 1) \quad (3)$$

Here, i_s is the diode saturation current, α is the diode slope parameter, and $V = V_c \cos(\omega_c t) + v_{\text{neuro}} \cos(\omega_{\text{neuro}} t)$ is the known applied signal voltage across the diode pair (V_c is the large signal carrier voltage amplitude and v_{neuro} is the small signal neural voltage amplitude). From (2) and (3), the conductance for each diode is given by

$$g_1 = \frac{di_1}{dV} = \alpha i_s e^{-\alpha V} \quad (4)$$

$$g_2 = \frac{di_2}{dV} = \alpha i_s e^{\alpha V} \quad (5)$$

Combining (4) and (5), the effective conductance of the APDP is then given by

$$g = g_1 + g_2 = \alpha i_s (e^{\alpha V} + e^{-\alpha V}) = 2\alpha i_s \cosh \alpha V \quad (6)$$

In evaluating the effective conductance, v_{neuro} is assumed to be sufficiently small. It follows that g is determined only by the biasing large signal V_c . By expanding the Taylor series of $\cosh \alpha V$:

$$\begin{aligned} g &= 2\alpha i_s [I_0(\alpha V_c) + 2I_2(\alpha V_c) \cos 2\omega_c t + \\ &\quad + 2I_4(\alpha V_c) \cos 4\omega_c t + \dots] \end{aligned} \quad (7)$$

where $I_n(\alpha V_c)$ are the modified Bessel functions of the second kind [31]-[33].

The instantaneous current through the APDP can then be estimated by:

$$\begin{aligned}
 i &= i_1 + i_2 = gV = \\
 &= g(V_c \cos(\omega_c t) + v_{neuro} \cos(\omega_{neuro} t)) = \\
 &= A1 \cos(\omega_{neuro} t) + \\
 &\quad B1 \cos(\omega_c t) + B2 \cos(3\omega_c t) + \dots + \\
 &\quad C1 \cos(2\omega_c \pm \omega_{neuro} t) + \\
 &\quad C2 \cos(4\omega_c \pm \omega_{neuro} t) + \dots
 \end{aligned} \tag{8}$$

where $A1$, $B1$, etc. are the coefficients based on the Taylor series expansion and which are a function of V_c , v_{neuro} , and g (see (7)).

Some observations/conclusions from (8) are: (a) only odd-order harmonics are present ($2f_c \pm f_{neuro}$ for this case), and (b) no DC term exists. The latter is crucial in avoiding DC currents that could potentially flow through the brain and harm the neurons. It is also noted that the undesirable DC term, and the even-order products are ideally kept within the diode pair loop (see Fig. 2) and never exit the circuit [31]-[33].

The aforementioned analysis is, of course, based on ideal circuit components, where diodes D1 and D2 are identical, i.e., they have the same saturation current, i_s , and slope parameter, α [32]. In an actual scenario, a slight mismatch between the diodes will be seen. Therefore, some very low DC component and odd harmonic mixing products will eventually appear at the APDP output. To minimize these undesirable effects, (commercially available) packaged APDP was used. The latter are better matched as the diodes' tolerances are kept at smaller percentages.

2) Implanted mixer performance

A wired APDP circuit was first designed and tested to assess the performance of the implanted mixer independent of losses created by the tissue environment and the wireless transmission through this medium. The circuit design is shown in Fig. 3(a). For this wired set-up, the 2.4 GHz carrier signal reaches the mixer through a circulator. Also, the neural signals at f_{neuro} are generated by a function generator. The goal is to detect the generated mixing products through a spectrum analyzer connected to the circuit through the circulator. As seen in Fig. 3, the testing circuit is comprised of the following: (a) anti-parallel diode pair (APDP) that mixes the carrier signal at 2.4 GHz with the recorded neural signals at f_{neuro} , (b) capacitor, $C1 = 1$ nF, that accounts for the bypass capacitor of Fig. 1, and (c) pair of capacitors ($C2 = 1$ μ F, $C3 = 0.4$ pF) used to match the mixer's high-frequency port to 50 Ω .

The fabricated mixer prototype corresponding to the setup in Fig. 3(a) is depicted in Fig. 3(b). It is printed on a 31 mils (0.79 mm) FR-4 ($\epsilon_r = 4.6$, $\tan\delta = 0.016$) substrate and has dimensions $L_m = 21.9$ mm, $W_m = 15$ mm and $H_m = 0.79$ mm. To improve matching between the mixer diodes, a packaged low barrier Schottky APDP from AVAGO Technologies (HSMS-286C) was used. The low-barrier Schottky diodes were selected because they have low saturation current, implying low turn-on voltage. This is important for: (a) avoiding additional biasing circuits that increase design

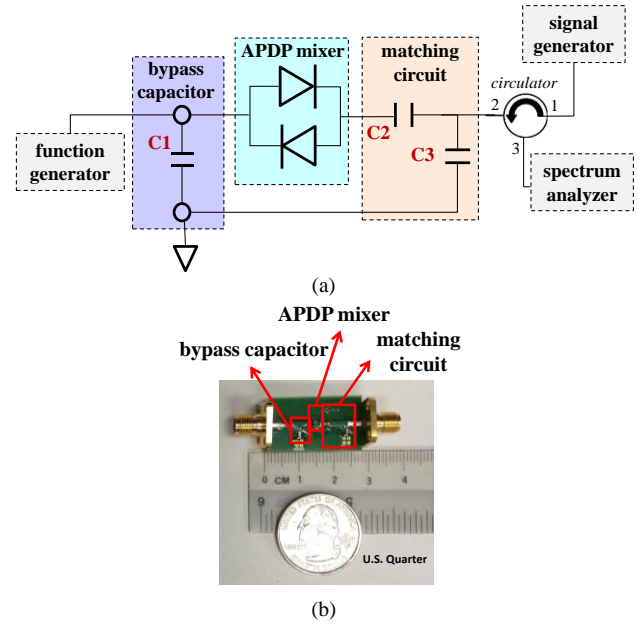


Fig. 3. Proposed implanted mixer circuit in wired configuration: (a) test bench ($C1 = 1$ nF, $C2 = 1$ μ F, $C3 = 0.4$ pF), and (b) fabricated prototype.

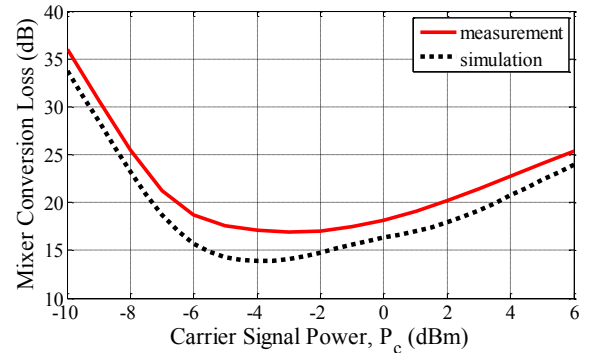


Fig. 4. Conversion loss of the mixer circuit in wired configuration as a function of the carrier signal power, P_c ($f_{neuro} = 1$ kHz, $P_{neuro} = -40$ dBm).

complexity, and (b) having diodes that turn “ON” under low carrier signal power. The latter is important in keeping the tissue-induced Specific Absorption Rate (SAR) within the safety limits imposed by international guidelines by limiting supplied carrier power [34] [35].

Harmonic balance simulations were carried out in Agilent® Advanced Design System (ADS) to model the diodes using SPICE model parameters (from vendor datasheet). To improve the simulations accuracy, electromagnetic (EM) co-simulations were included with ADS for the microstrip lines surrounding the diodes and the capacitors.

The mixer performance was assessed in terms of its exhibited conversion loss. For this case, it is defined as the ratio of the neural signal (f_{neuro}) power at the terminals of the bypass capacitor (see Fig. 1) to the received modulated signal power at 4.8 GHz $\pm f_{neuro}$. That is:

$$\begin{aligned}
 \text{Mixer Conversion Loss (dB)} &= \\
 &= P_{neuro} \text{ (dBm)} - P_{Rx@4.8GHz \pm f_{neuro}} \text{ (dBm)}
 \end{aligned} \tag{9}$$

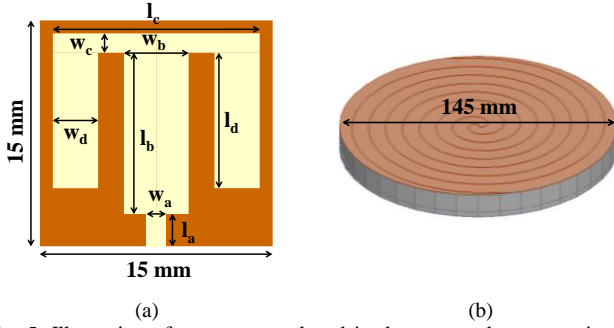


Fig. 5. Illustration of antennas employed in the proposed neurosensing system: (a) implanted patch antenna, and (b) exterior interrogator spiral antenna.

TABLE II
DIMENSIONS OF THE IMPLANTED PATCH ANTENNA IN FIG. 5

Parameter	Dimension (mm)
w_a	1.37
l_a	2.00
w_b	4.23
l_b	11.07
w_c	1.29
l_c	13.61
w_d	2.95
l_d	9.18

Fig. 4 gives the simulated vs. measured conversion loss, indicating good agreement. Specifically, Fig. 4 plots the mixer conversion loss as a function of the 2.4 GHz carrier signal power, P_c . This is done for neural signals at $f_{\text{neuro}} = 1$ kHz having a power of $P_{\text{neuro}} = -40$ dBm. As seen, the mixer conversion loss is minimum when $P_c = -4$ dBm. A discrepancy of approximately 3.2 dB is observed between simulations and measurements. This is most likely due to packaging losses or differences between the D1 and D2 diodes. Regardless, the measured conversion loss of the mixer circuit at $f_{\text{neuro}} = 1$ kHz of 17.1 dB meets the design specification of < 25 dB.

B. Antennas

1) Antenna design

The implanted and interrogator antennas are specifically designed to exhibit good electromagnetic (EM) coupling in the near field. The goal is to achieve high transmission coefficient, $|S_{21}|$, at both 2.4 GHz and 4.8 GHz, for a distance of approximately 8 mm between the antennas. This distance accounts for the head tissue layers (dura, skull, and skin) that would lie between the implant and the external interrogator. High $|S_{21}|$ at 4.8 GHz reduces the overall loss on the recorded neural signals, thus improving the system sensitivity. High $|S_{21}|$ at 2.4 GHz implies that the minimum carrier signal power to turn “ON” the mixer diodes will be low as well. This is also important for preserving patient safety against EM fields [34] [35]. In the following, simulations are carried out using ANSYS® High Frequency Structure Simulator (HFSS), and compared with measurements.

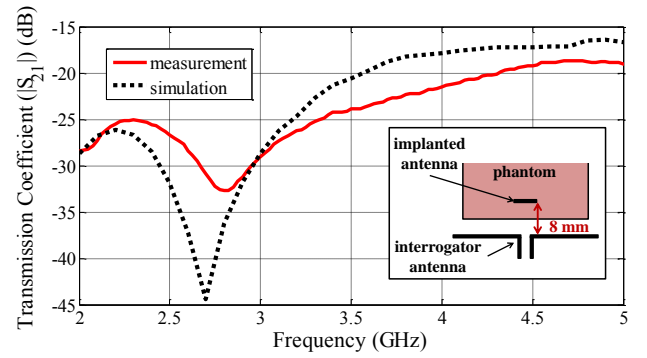


Fig. 6. Simulated vs. measured transmission coefficient, $|S_{21}|$, between the implanted and interrogator antennas. The employed set-up is shown in the inset (inset not to scale).

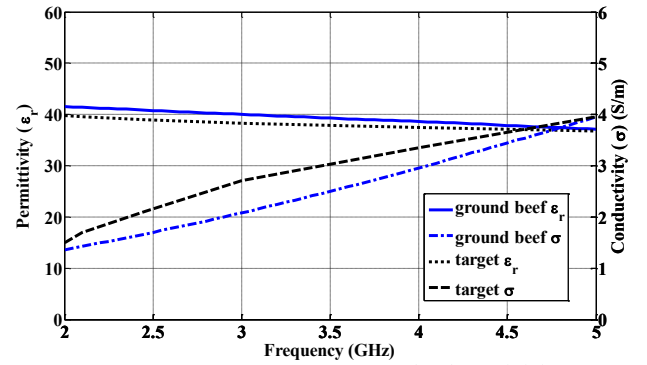


Fig. 7. Theoretical [41] vs. measured average head permittivity (ϵ_r) and conductivity (σ).

The design of the proposed dual-band (2.4/4.8 GHz) implanted patch antenna is shown in Fig. 5(a). It is printed on a 31 mils (0.79 mm) FR-4 substrate ($\epsilon_r = 4.6$, $\tan\delta = 0.016$) and has dimensions $L_a = 15$ mm, $W_a = 15$ mm and $H_a = 0.79$ mm. This implanted antenna is covered with a 0.7 mm-thick polydimethylsiloxane (PDMS) layer ($\epsilon_r = 2.8$, $\tan\delta = 0.001$ [36]). This superstrate serves to preserve the biocompatibility of the antenna by insulating its metallization from the surrounding biological tissues [37]. Additionally, this relatively lossless insulation reduces the power absorbed by the human body, and increases the antenna’s efficiency [38] [39]. The rest of the antenna dimensions are given in Table II.

The design of the employed spiral interrogator antenna is shown in Fig. 5(b). It is a low-profile ultra wide-band slot spiral antenna. The diameter of the spiral is 145 mm, and operates from 0.6 GHz to 6 GHz [28] [29]. The low-profile property of this spiral antenna enhances its near field coupling with the implanted patch antenna, thus allowing for high transmission coefficient, $|S_{21}|$, between the two.

2) Antenna Performance

Simulated vs. measured data for the transmission coefficient, $|S_{21}|$, between the implanted and interrogator antennas are given in Fig. 6. The employed set-up is shown in the inset of Fig. 6. The implanted antenna is placed inside a head-equivalent phantom. The interrogator antenna is placed right outside the phantom, at a distance of 8mm from the implanted antenna.

As depicted in Fig. 6, at 4.8 GHz, the retransmitted $|S_{21}|$ is measured to be 19 dB. This meets the design specification of < 25 dB. At 2.4 GHz, $|S_{21}|$ is measured to be 26 dB. This means that, for an intended carrier having signal power of $P_c = -4$ dBm impinging upon the implanted antenna (see Fig. 4), the power transmitted by the interrogator will be ~ 22 dBm. As would be expected, differences between simulations and measurements are likely due to possible fabrication errors of the implanted and interrogator antennas and due to discrepancies in the electrical properties of the phantom (see Fig. 7).

C. Phantom Modeling and Specific Absorption Rate (SAR)

Simulations were carried out for the implanted antenna while immersed inside a single-layer tissue model (see inset of Fig. 6). For these simulations, the average head dielectric properties listed in [40] [41] were used. As indicated in Fig. 7, the permittivity and conductivity of the human head (“target”) [40] are well represented by the chosen ground beef properties used in measurements. The latter consisted of 80% lean meat and 20% fat. This ratio was found to have the closest match to the intended “target” dielectric properties. Permittivity and conductivity of the employed phantom were measured using the Agilent® 85070E Dielectric Probe Kit to ensure correspondence with the simulation. During these measurements, we ensured that air gaps within the ground beef were minimized (otherwise the permittivity and conductivity will be lower). Also, during measurements, the beef phantom was placed inside a 0.3 mm-thick polypropylene container (see Fig. 8). We remark that single-layer head phantoms were also employed for brain implant studies in [11] [12]. In the future, the proposed implant will be tested within a multi-layer head phantom, similar to the set-up employed in [15] [42].

Preliminary SAR studies were also performed for this proof-of-concept neurosensing system. Simulation showed that the employed interrogator power of ~ 20 dBm satisfied the FCC [34] and IEEE C95.1-2005 [35] guidelines for controlled environment exposure.

IV. NEUROSENSING SYSTEM PERFORMANCE

The measurement set-up used to assess the performance of the overall wireless neurosensing system is shown in Fig. 8. The implant is comprised of both the implanted mixer and the antenna. Currently, its dimensions are $L_s = 36.9$ mm, $W_s = 15$ mm and $H_s = 0.79$ mm. It is immersed inside a ground beef phantom that emulates the average dielectric properties of the head’s tissue [41] (see Fig. 7). The goal is to emulate the surrounding head tissues on the implant’s performance in a realistic scenario.

The interrogator spiral is placed right outside the phantom, and at a distance of 8 mm from the implant. The 2.4 GHz carrier signal (power of ~ 20 dBm) reaches the interrogator antenna through a circulator. It is then transmitted wirelessly to the implanted antenna for activation of the neurosensor. A function generator is also used to emulate neural signals at f_{neuro} . For this proof of concept experiment, an SMA connector

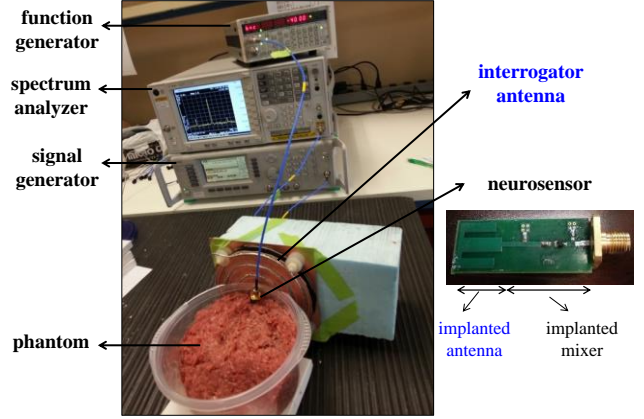


Fig. 8. Measurement set-up used to test the performance of the overall neurosensing system in wireless configuration.

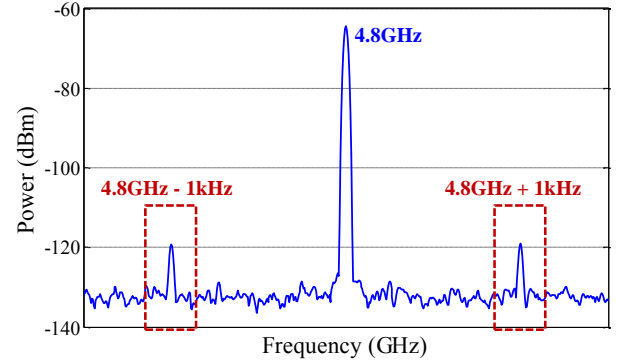


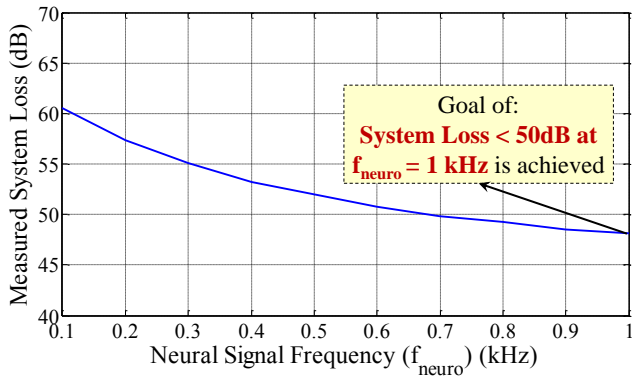
Fig. 9. Example measured spectral response of the proposed neurosystem in wireless configuration ($f_{\text{neuro}} = 1$ kHz, $P_{\text{neuro}} = -70$ dBm).

connected the implant to the function generator via a coaxial cable. The neural signals are mixed with the wirelessly supplied carrier to generate and backscatter signals at $4.8 \text{ GHz} \pm f_{\text{neuro}}$. Subsequently, the modulated signal is wirelessly received by the interrogator antenna. It is then detected through a spectrum analyzer. For example, Fig. 9 shows the measured spectral response of the neurosensing system when $f_{\text{neuro}} = 1$ kHz and $P_{\text{neuro}} = -70$ dBm, which corresponds to a neural signal voltage of $200 \mu\text{V}_{\text{pp}}$. The sidebands associated with the recorded neural signals ($4.8 \text{ GHz} \pm 1 \text{ kHz}$) are indicated in red.

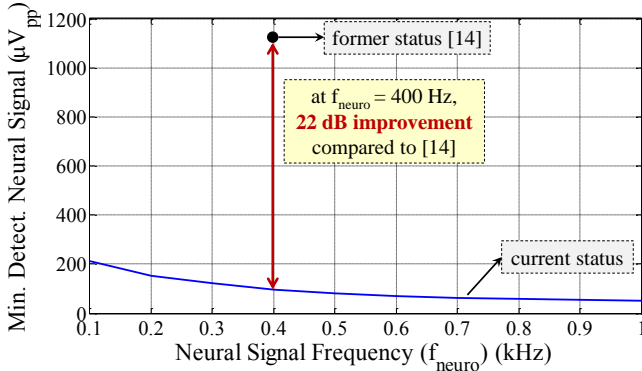
The measured system loss as a function of f_{neuro} is shown in Fig. 10(a). Similarly to (9), loss is defined as the ratio of the neural signal power at the terminals of the bypass capacitor (see Fig. 1) to the power of the received modulated ($4.8 \text{ GHz} \pm f_{\text{neuro}}$) signal at the interrogator side; this is distinguished by the previous conversion loss in (9) in that here the wireless propagation and antenna losses are incorporated. Therefore:

$$\begin{aligned} \text{System Loss (dB)} &= \\ &= P_{\text{neuro}} \text{ (dBm)} - P_{\text{Rx}@ (4.8\text{GHz} \pm f_{\text{neuro}})} \text{ (dBm)} \end{aligned} \quad (10)$$

Misalignment losses between the implanted and interrogator antennas were also addressed. Specifically, full-wave



(a)



(b)

Fig. 10. Minimum detectable neural signal levels: (a) measured system loss as a function of f_{neuro} , and (b) minimum detectable neural signal as a function of f_{neuro} (assuming $\text{MDS}_{\text{Rx}} = -130$ dBm, as indicated in (1)).

simulations (see Fig. 11) showed that the worst case deterioration in system loss for ± 1 cm misalignment is ~ 7 dB. This ± 1 cm misalignment was assumed to be the maximum offset allowable by the interrogator antenna embedded within a baseball cap.

The minimum neural signals to be detected using the proposed neurosystem are shown in Fig. 10(b). These curves are subject to the minimum detectable signal (MDS_{Rx}) of -130 dBm at the spectrum analyzer. As can be seen in Fig. 10(a), the system loss at $f_{\text{neuro}} = 1$ kHz of 48 dB meets the design specification of < 50 dB. Specifically, neural signals as low as -82 dBm ($\sim 50 \mu\text{V}_{\text{pp}}$) can be detected at $f_{\text{neuro}} = 1$ kHz. Additionally, neural signals as low as -70 dBm ($200 \mu\text{V}_{\text{pp}}$) can be detected at $f_{\text{neuro}} = 100$ Hz. Of course, neural signals lower than $50 \mu\text{V}_{\text{pp}}$ can be detected at $f_{\text{neuro}} > 1$ kHz. Remarkably, the sensitivity of the proposed system is up to 22 dB higher than that reported in [14]. Specifically, at $f_{\text{neuro}} = 400$ Hz, the minimum neural signal detected by the developed system is -77 dBm, viz. 22 dB lower than that reported in [14].

Overall, the proposed neurosensing system can read (see Table 1): (a) all ECoG signals across a 300 – 500 Hz bandwidth, (b) all neural “spikes” across the theoretical 300 Hz – 5 kHz bandwidth, and (c) LFPs of $> 200 \mu\text{V}_{\text{pp}}$ across a 100 – 500 Hz bandwidth. This remarkable high sensitivity brings forward a new possibility of wireless neural signal detection using passive brain implant topologies.

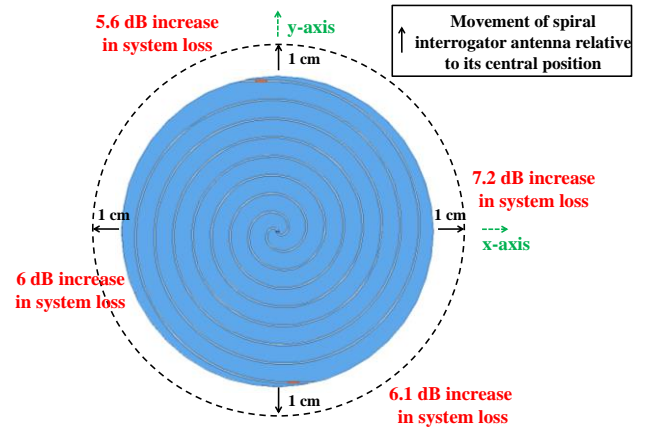


Fig. 11. System losses due to misalignments of ± 1 cm between the interrogator and implant (see Fig. 7, inset).

V. CONCLUSION

A high-sensitivity, fully-passive neurosensing system was presented for wireless brain signal monitoring. This system is able to detect very low voltage brain-like signals. Specifically, the proposed system was demonstrated to read emulated neural signals as low as -82 dBm ($50 \mu\text{V}_{\text{pp}}$) at $f_{\text{neuro}} > 1$ kHz. It was shown that neural signals as low as -70 dBm ($200 \mu\text{V}_{\text{pp}}$) for $f_{\text{neuro}} > 100$ Hz can also be detected. This is an improvement of up to 22 dB in sensitivity as compared to [14]. The neurosensing system was comprised of an implanted neurosensor and an exterior interrogator. The neurosensor receives a carrier signal and mixes it with the emulated neural signals. The mixing components are then retransmitted back to the interrogator. To lower losses, the system employed: (a) a sub-harmonic mixer with anti-parallel diode pair (APDP), (b) a pair of implanted/interrogator antennas with high transmission coefficient, $|S_{21}|$, and (c) a matching circuit between the implanted antenna and mixer. Of importance is that the proposed system is fully-passive and wireless. As such, it can allow for continuous and unobtrusive monitoring of brain signals with minimum impact to the individual’s activity.

At this stage, the high sensitivity of the proposed neurosensing system brings forward new possibilities for wireless neural signal detection using passive brain implants. Example applications include but not limited to: 1) early detection of epileptic seizures, 2) behavioral studies to assess levels of consciousness (e.g., during sleep, anesthesia or brain injury), 3) understanding and improving the brain’s functionality for the aging, people with Alzheimer’s and people with mental disorders, etc. There is, of course, a need to further reduce the implant size and signal detection sensitivity. With this in mind, in the future, the following research steps will be pursued: (a) Temporal waveform acquisition, (b) In-vivo evaluation, (c) Implant miniaturization (e.g., higher permittivity substrates and/or MEMS fabrication techniques, etc), (d) Further improvement of the system’s neural signal detection sensitivity to detect all brain signals in Table I, (e) Improve implant biocompatibility and flexibility (e.g., polyimide or parylene substrates to fabricate the

implanted sensor and antenna), (f) Introduce multi-channel sensing for multiple signal detection, and (g) Body Area Network implementation.

ACKNOWLEDGMENT

The authors would like to thank Helen Schwerdt for her advice and suggestions for the course of this research.

REFERENCES

- [1] M.J. During, A. Freese, B.A. Sabel, W.M. Saltzman, A. Deutch, R.H. Roth, and R. Langer, "Controlled release of dopamine from a polymeric brain implant: in vivo characterization," *Ann. Neurol.*, vol. 25, no. 4, pp. 351-56, 1989.
- [2] V.S. Polikov, P.A. Tresco, and W.M. Reichert, "Response of brain tissue to chronically implanted neural electrodes," *J. Neurosci. Meth.*, vol. 148, pp. 1-18, 2005.
- [3] J.P. Blount, J. Cormier, H. Kim, P. Kankirawatana, K.O. Riley, and R.C. Knowlton, "Advances in intracranial monitoring," *Neurosurg. Focus*, vol. 25, no. 3, pp. 1-8, Sept. 2008.
- [4] L.R. Hochberg, M.D. Serruya, G.M. Friebs, J.A. Mukand, M. Saleh, A.H. Caplan, A. Branner, G. Chen, R.D. Penn and J.P. Donoghue, "Neuronal ensemble control of prosthetic devices by a human with tetraplegia," *Nature*, vol. 442, no. 7099, pp. 164-171, 2006.
- [5] D.R. Kipke, W. Shain, G. Buzsaki, E. Fetz, J.M. Henderson, J.F. Hetke, and G. Schalk. "Advanced neurotechnologies for chronic neural interfaces: new horizons and clinical opportunities," *J. Neurosci.*, vol. 28, no. 46, pp. 11830-11838, 2008.
- [6] K.D. Wise, "Microelectrodes, microelectronics, and implantable neural microsystems," *Proc. IEEE*, vol. 96, no. 7, pp. 1184-1202, Jul. 2008.
- [7] A. Waziri, C.A. Schevon, J. Cappell, R.G. Emerson, G.M. McKhann, and R.R. Goodman. "Initial surgical experience with a dense cortical microarray in epileptic patients undergoing craniotomy for subdural electrode implantation," *Neurosurg.*, vol. 64m pp. 540-545, 2009.
- [8] J.C. LaManna, K.A. McCracken, M. Patil, and O.J. Prohaska, "Stimulus-activated changes in brain tissue temperature in the anesthetized rat," *Metab. Brain Disease*, vol. 4, pp. 225-237, 1989.
- [9] J. Dethier, P. Nuyujukian, S.I. Ryu, K.V. Shenoy, and K. Boahen, "Design and validation of a real-time spiking-neural-network decoder for brain-machine interfaces," *J. Neur. Eng.*, vol. 10, no. 3, 2013.
- [10] A. Dementyev and J.R. Smith, "A wearable UHF RFID-based EEG system," in *Proc. IEEE Int. Conf. RFID*, 2013
- [11] E. Moradi, T. Bjorninen, L. Sydanheimo, J. M. Carmena, J. M. Rabaey, and L. Ukkonen, "Measurement of wireless link for brain-machine interface systems using human-head equivalent liquid," *IEEE Antennas Wireless Propag. Lett.*, vol. 12, pp. 1307-1310, 2013.
- [12] E. Moradi, K. Koski, T. Bjorninen, L. Sydanheimo, J. M. Rabaey, J. M. Carmena, Y. Rahmat-Samii, and L. Ukkonen, "Miniature implantable and wearable on-body antennas: towards the new era of wireless body-centric systems," *IEEE Antennas Propag. Magazine*, vol. 56, no. 1, pp. 271-291, Feb. 2014.
- [13] G. Schalk and E.C. Leuthardt, "Brain-computer interfaces using electrocorticographic signals," *IEEE Rev. Biomed. Eng.*, vol. 4, pp. 140-154, 2011.
- [14] H.N. Schwerdt, W. Xu, S. Shekhar, A. Abbaspour-Tamijani, B.C. Towe, F.A. Miranda, and J. Chae, "A fully passive wireless microsystem for recording of neuropotentials using RF backscattering methods," *J. Microelectromech. Syst.*, vol. 20, pp. 1119-1130, Oct. 2011.
- [15] H.N. Schwerdt, F.A. Miranda, and J. Chae, "A fully passive wireless backscattering neurorecording microsystem embedded in dispersive human-head phantom medium," *IEEE Electron. Dev. Lett.*, vol. 33, no. 6, pp. 908-910, Jun. 2012.
- [16] G. Schalk and E.C. Leuthardt, "Brain-computer interfaces using electrocorticographic signals," *IEEE Rev. Biomed. Eng.*, vol. 4, pp. 140-154, 2011.
- [17] R. R. Harrison, "Design of integrated circuits to observe brain activity," *Proc. IEEE*, vol. 96, no. 7, pp. 1203-1216, Jul. 2008.
- [18] R.R. Harrison, "A versatile integrated circuit for the acquisition of biopotentials," in *Proc. IEEE Custom Integr. Circ. Conf.*, pp. 115-122, 2007.
- [19] S.P. Burns, D. Xing, and R.M. Shapley, "Comparisons of the dynamics of local field potential and multiunit activity signals in macaque visual cortex," *J. Neurosci.*, vol. 30, no. 41, pp. 13739-13749, Oct. 2010.
- [20] C. Lee, A. Kiourti, J. Chae, and J.L. Volakis, "Fully-passive and wireless detection of very-low-power brain signals," in *Proc. IEEE MTT-S Int. Microw. Workshop Series on RF and Wireless Technol. for Biomed. and Healthcare Appl.*, London, UK, Dec. 2014.
- [21] A. Kiourti, Z. Wang, C. Lee, H. Schwerdt, J. Chae, and J.L. Volakis, "A wireless neurosensing system for remote monitoring of brain signals," in *Proc. 8th Europ. Conf. Antennas Propag.*, The Hague, The Netherlands, 2014.
- [22] A. Kiourti, C. Lee, A. Akhiyat, H. Schwerdt, J. Chae, and J.L. Volakis, "Passive, on chip and in situ detection of neuropotentials," in *Proc. IEEE Int. Symp. Antennas Propag.*, Memphis, TN, 2014.
- [23] H.N. Schwerdt, F.A. Miranda, and J. Chae, "Analysis of electromagnetic fields induced in operation of a wireless fully passive backscattering neurorecording microsystem in emulated human head tissue," *IEEE Trans. Microw. Theory Techn.*, vol. 61, no. 5, pp. 2170-2176, May 2013.
- [24] "International Telecommunication Union-Radiocommunications (ITU-R), radio regulations, section 5.138 and 5.150," ITU. Geneva, Switzerland.
- [25] J. Shefer and H. Staras, "Harmonic radar detecting and ranging system for automotive vehicles," U.S. Patent 3781879 A, Dec. 25, 1973.
- [26] B.G. Colpitts and G. Boiteau, "Harmonic radar transceiver design: miniature tags for insect tracking," *IEEE Trans. Antennas Propag.*, vol. 52, no. 11, pp. 2825-2832, Nov. 2004.
- [27] G.A. Vera, Y. Duroc, and S. Tedjini, "Analysis of harmonics in UHF RFID signals," *IEEE Trans. Microw. Theory Techn.*, vol. 61, no. 6, pp. 2481-2490, Jun. 2013.
- [28] M.W. Nurnberger and J.L. Volakis, "A new planar feed for slot spiral antennas," *IEEE Trans. Antennas Propag.*, vol. 44, no. 1, Jan. 1996.
- [29] B.A. Kramer, C.C. Chen, and J.L. Volakis, "Size reduction of a low-profile spiral antenna using inductive and dielectric loading," *IEEE Antennas Wireless Propag. Lett.*, vol. 7, 2008.
- [30] C. Drentea, *Modern Communications Receiver Design and Technology*, Norwood, MA, Artech House, 2010.
- [31] B. R. Jackson, "Subharmonic mixers in CMOS microwave integrated circuits," Ph.D dissertation, Dept. of Elect. and Comp. Eng., Queen's Univ., Ontario, Canada, 2009.
- [32] M. Merwe and JB Swardt, "The design and evaluation of a harmonic mixer using an anti-parallel diode pair," AWR Corp. Application Note, El Segundo, CA.
- [33] E. Camargo, *Design of FET frequency multipliers and harmonic oscillators*. Artech House Publishers:1998.
- [34] *Evaluating Compliance with FCC Guidelines for Human Exposure to Radio Frequency Electromagnetic Fields*, FCC OET Bulletin.65, Washington D.C., August 1997.
- [35] *IEEE Standard for Safety Levels With Respect to Human Exposure to Radiofrequency Electromagnetic Fields, 3 kHz to 300 GHz*, IEEE Standard C95.1, 2005.
- [36] S. Koulouridis, G. Kiziltas, Y. Zhou, D.J. Hansford, and J.L. Volakis, "Polymer-ceramic composites for microwave applications: fabrication and performance assessment," *IEEE Microw. Theory Techn.*, vol. 54, no. 12, pp. 4202-4208, Dec. 2006.
- [37] A. Kiourti and K.S. Nikita, "Implantable antennas: a tutorial on design, fabrication, and in vitro/in vivo testing," *IEEE Microwave Magazine*, vol. 15, no. 4, pp. 77-91, Jun. 2014.
- [38] F. Merli, B. Fuchs, J. R. Mosig, and A.K. Skrivervik, "The effect of insulating layers on the performance of implanted antennas," *IEEE Trans. Antennas Propag.*, vol. 59, no. 1, Jan. 2011.
- [39] F. Merli, B. Fuchs, and A.K. Skrivervik, "Influence of insulation for implanted antennas," in *Proc. 3rd Europ. Conf. Antennas Propag.*, 2009.
- [40] S. Gabriel, R. W. Lau, and C. Gabriel, "The dielectric properties of biological tissues: II. Measurements in the frequency range 10 Hz to 20 GHz," *Phys. Med. Biol.*, vol. 41, pp. 2251-2269, 1996.
- [41] CTIA Certification Standard "Test Plan for Wireless Device Over-the-Air Performance," Revision 3.3, Oct. 2013.
- [42] R. Warty, M-R. Tofighi, U. Kawoos, and A. Rosen, "Characterization of implantable antennas for intracranial pressure monitoring: Reflection by and transmission through a scalp phantom," *IEEE Microw. Theory Techn.*, vol. 56, no. 10, pp. 2366-2376, Oct. 2008.